Design of large-area metasurfaces for the mid-IR and suited for CMOS-compatible fabrication by masked lithography

Wolffenbuttel, Reinoud F.; Ghaderi, M. Amir

DOI
10.1016/j.photonics.2022.101050

Publication date
2022

Document Version
Final published version

Published in
Photonics and Nanostructures - Fundamentals and Applications

Photonics and Nanostructures - Fundamentals and Applications 51 (2022) 101050

Contents lists available at ScienceDirect

Photonics and Nanostructures - Fundamentals and Applications

journal homepage: www.elsevier.com/locate/photonics

Design of large-area metasurfaces for the mid-IR and suited for CMOS-compatible fabrication by masked lithography

Reinoud F. Wolffenbuttel [a,*], M. Amir Ghaderi [a]

[a] Laboratory for Electronic Instrumentation, Department of Microelectronics, Delft University of Technology, 2628 CD Delft, the Netherlands

ARTICLE INFO

Keywords:
Mid-infrared sensing
Metamaterial absorber
Metasurface
MEMS technology
CMOS compatibility

ABSTRACT

The use of masked UV (i-line) lithography in a MEMS foundry for CMOS-compatible fabrication of large-area metasurface-based absorbers for the mid-infrared is demonstrated. The challenges are in: (a) the limited number of acceptable metals, (b) the thickness tolerance of the layers used in the CMOS process, and (c) the imaging capabilities of i-line lithography as compared to e-beam. The claimed throughput advantage with manageable distortion of masked lithography and the suitability of the layers used in a CMOS-compatible process in the fabrication of mid-IR absorbers was tested. Issues investigated are: (a) the impact of aluminium as the preferred metal in the MIM patch on the plasmonic response, (b) the influence of SiO_2 as preferred dielectric material, (c) the effect of corner rounding and horizontal-vertical bias of the masked lithography and (d) measures that can be taken during the design phase to mitigate any such detrimental effect. Based on the findings, disk-shaped patches are identified as the most suitable for shape-tolerant design. Metasurfaces with a unit-cell side-length of $3\mu m$ were fabricated over a chip area larger than $10^5\mu m^2$. Measurements do confirm that (a) aluminium is a suitable CMOS-compatible material for mid-IR metamaterial absorber fabrication, (b) a large surface roughness results in widening of the absorption peaks and (c) the typical layer thickness tolerance used in a MEMS foundry is also acceptable for mid-IR metasurface fabrication. Masked lithography limits the minimum design wavelength to about $3.5\mu m$, while the surface roughness $Rq \sim 5nm$ results in a bandwidth up to $FWHM = 400nm$.

1. Introduction

1.1. Background

Metamaterial absorbers are based on an array of unit cells. Often each cell is composed of a metal-insulator-metal (MIM) stack, with the top metal patterned into a patch of sub-wavelength dimensions and the back-metal layer acting as a ground shield, thus preventing any transmission into the underlying substrate [1]. A near-unity absorbance is achieved when the impedance of the absorber matches to that of the free-space, which results in principle in a perfectly non-reflective surface. The impedance of the metamaterial absorber can be tuned by the dimensions and shape of the pattern in the MIM structures [2,3]. Both the electric and magnetic responses are simultaneously controlled by engineering of the details of the inner structure of this unit cell. Therefore, the photonic response critically depends on the control of the dimensions of the features while fabricated.

The side-length of the unit cell is usually slightly smaller than the wavelength and is in the $2-4\mu m$ range in case of operation in the mid-IR. Each unit cell contains an inner fine pattern with sub-wavelength features. Although masked lithography would in principle allow full wafer coverage In sensor applications a large array of identical unit cells is required over an absorber area of $0.1mm^2$ typically and up to $1mm^2$ to ensure that (a) an impinging beam spot of practical diameter is covered and (b) the absorber extends over the underlying microfabricated detector [2,3]. The ratio between the overall dimensions and the minimum feature size makes such an absorber a 'large area' device, which has a profound effect on the choice of the most-suitable lithography system to be used.

Metamaterial-based absorbers for the near/mid-IR require a unit-cell with a minimum feature size that is comparable to that of structures fabricated in microelectronics, thus similar fabrication techniques can be applied. The basic scaling factor in metamaterial absorber design is the design wavelength (center wavelength), λ_o, which in a first approximation determines the side-length of the unit-cell, while the complexity of the absorber design, in terms of for instance the bandwidth relative to λ_o, largely defines the feature size of the structure within the unit cell. Therefore, the requirements on resolving power of

* Corresponding author.
E-mail address: r.f.wolffenbuttel@tudelft.nl (R.F. Wolffenbuttel).

https://doi.org/10.1016/j.photonics.2022.101050
Received 19 February 2022; Received in revised form 19 July 2022; Accepted 1 August 2022
Available online 4 August 2022

the lithography system increase with decreasing center wavelength and with the complexity of the design. For this reason, high-resolution lithography methods, such as e-beam [4,5], deep ultra-violet (DUV) [6], or direct laser write [7] lithography are used for absorbers operating at mid-IR and near-IR spectra. The trade-off between throughput and feature size is in e-beam lithography clearly skewed towards the latter, as its capabilities on minimum feature size are amply sufficient to yield structures of sub-wavelength dimensions, while the sequential 'writing' of the patterns is time consuming. Nanoimprinting [8] and techniques involving laser interference [9] have been used for the fabrication of metasurfaces with higher throughput over large areas. However, these are difficult to implement in a CMOS-compatible fashion.

Although an integrated gas sensor with a metasurface-coated thermal emitter and thermal detector fabricated in CMOS using e-beam has been reported [5,10], in general the high-throughput challenge favors the use of masked lithography [11]. CMOS-compatible micro electro mechanical system (MEMS)-technology is mainly driven by its potential for low unit cost at the high-volume fabrication that wafer-level fabrication can bring. Consequently, throughput is an important consideration. Applying UV (i-line) lithography to the definition of sub-wavelength features is challenging in case of absorber fabrication for the mid-IR when considering the minimum feature size of about $350nm$. Its successor, DUV lithography, is still considered prohibitively expensive in a foundry dedicated to MEMS fabrication. Although masked lithography would in principle allow full wafer coverage with a metasurface, this paper is focused on CMOS-compatible fabrication of sensor systems that include absorbers with an area in the range of $0.1 - 1mm^2$.

1.2. Specific aims and organisation of the paper

Within the framework of this paper, the metamaterial is assumed to be part of a microsystem. The targeted field of application is integrated silicon sensors. Therefore, the constraints of masked UV (i-line) lithography (the state-of-the-art in the infrastructure of a MEMS cleanroom) has been explored here for mid-IR metamaterial absorber fabrication, despite the fact that this level of lithography is considered somewhat outdated in mainstream micro-electronics industry. The findings of this paper are expected to remain relevant, as the targeted improved minimum feature size on the IRDS photolithography roadmap [12] is likely to be exploited in the design of metamaterial-based absorbers by shifting the application domain from the mid-IR towards the visible. Therefore, the same limitation, albeit on a smaller measure of length, would re-appear in due course in the familiar quest for an ever-decreasing feature size.

The other constraint considered here also stems from the microsystem application field. The ambition for on-chip post-CMOS integration of sensor with circuits implies that absorber fabrication should be fully CMOS-compatible to ensure that the functionality of the already completed micro-electronic devices is not jeopardized. The CMOS-compatible fabrication of absorber subsequent to the detector integration implies that: (1) only a limited set of materials can be used and (2) processing is restricted to the acceptable techniques for layer deposition and etching. Moreover, (3) significantly increasing the accumulated temperature budget of already integrated micro-electronic devices by the thermal load by any subsequent MEMS process step is generally not acceptable.

A key objective of this work is to establish a shape-tolerant design methodology for the unit cell of metamaterial, for minimizing any detrimental effect of the limitations of masked lithography. The starting point is a two-dimensional array of metallic nanowires on top of a dielectric slab with a metallic ground plane. The excitation of free carriers in the metallic nanowire by the electric field of incident electromagnetic radiation creates a magnetic dipole moment, which cancels out the magnetic field component of the electromagnetic wave. Polarized light with its E field along the nanowire direction can, in principle, be perfectly absorbed [2,3]. The resonating wavelength (the wavelength with peak absorption) depends on the length of the wire, while the bandwidth of the absorption peak strongly depends on the electrical conductivity of the metal. A two-dimensional symmetric structure is required to eliminate the polarization dependence.

Three different geometries are generally considered. The cross-shaped structure is the most straightforward implementation and is essentially composed of two nanowires placed at perpendicular directions [13]. The squared structure (patch) is a special case of the cross, where the length of one of the nanowires equals the width of the other. Fabrication advantages can be expected, as the sharp inner corners are avoided. The circular disk (patch) operates using a similar principle, as it can be assumed a nanowire rotated around its center [4].

First, we discuss the choice of the metal for CMOS compatible patch fabrication, with an emphasis on the use of aluminium. Subsequently, the effects of the thickness tolerances, grain size, and roughness of the actual nanowire on the performance of the absorber are investigated. Furthermore, the effect of thickness tolerance in the spacer layer is investigated. Finally, the effect of shape tolerances of the structure within the unit-cell on the overall optical characteristics of the large-area absorber design are discussed. The simulations are validated using absorbers fabricated in a CMOS-compatible surface micromachining process.

Note that the simulations were done in COMSOL with postprocessing in MATLAB. A function from the MATLAB file exchange directory was used for analysing the permittivity of metals [14].

2. Analysis of key aspects of the metasurface design

2.1. Metals in CMOS-compatible metasurfaces

Gold (Au) and silver (Ag) are often the materials of choice as the plasmonic materials in state-of-the-art meta-material-based absorber designs, because of their high conductivity (hence high free carrier concentration) [3,4]. However, Au or Ag are generally regarded as sources of recombination centers in silicon and are often viewed with deep suspicion in a silicon cleanroom, which obviously hinders their implementation in a metamaterial-based absorber design for fabrication in CMOS-compatible MEMS. While aluminium (Al) is known as a rapidly diffusing acceptor dopant in silicon, it is nevertheless considered a more CMOS-compatible material. Al-based metamaterial absorbers have indeed been discussed in the literature, [11,13,15]. Other CMOS-compatible metals reported in the literature on metamaterial fabrication are copper [5] and tungsten [16].

An improved understanding of the limitations and opportunities of Al in plasmonic device design is essential when considering it as a competitive CMOS-compatible option. The Drude-based models are commonly used for describing the optical properties of metals by assuming a dielectric function with the vibration modes included as damped harmonic oscillators. The Brendel-Bormann (BB) model was found to give a better fit with experimental data on amorphous films and is based on the convolution of a Gaussian function with the Drude dielectric function [17]. The BB function also leads to a better fit in plasmonic applications and is used here to calculate the permittivity of the metals over the optical range [18].

Figure 1 a shows the optical properties of aluminium, gold, and silver over the mid-infrared range. Although the complex permittivity of Al is different from that of Au and Ag, the absorption characteristics of an optimized design of the metamaterial MIM structure in the respective material are highly similar, as shown in Figure 1b. The bandwidth of the absorber, which is specified in terms of the full width at its half-maximum (FWHM), is $292nm$ in the case of Al, which is just slightly larger than the FWHM of Au ($288nm$) and Ag ($272nm$).

The nominal thickness of the metal layer is not critical, but the electrical conductivity should be sufficient to avoid an adverse effect on the plasmonic response. The conductivity of bulk material is propor-

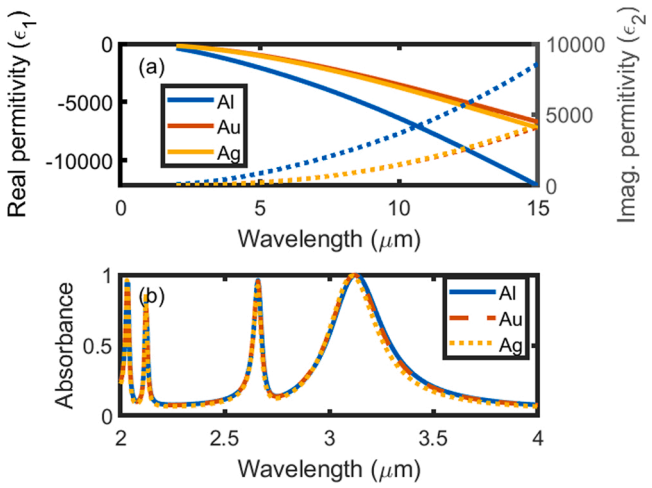

Fig. 1. (a) The real (solid lines) and imaginary (dotted lines) parts of the permittivity of Al, Au, and Ag calculated using BB model. (b) Simulated absorption peak for a disk-shaped metamaterial absorber with Al, silver (Ag), and gold (Au) for the disk-shaped patch of 1000*nm* diameter.

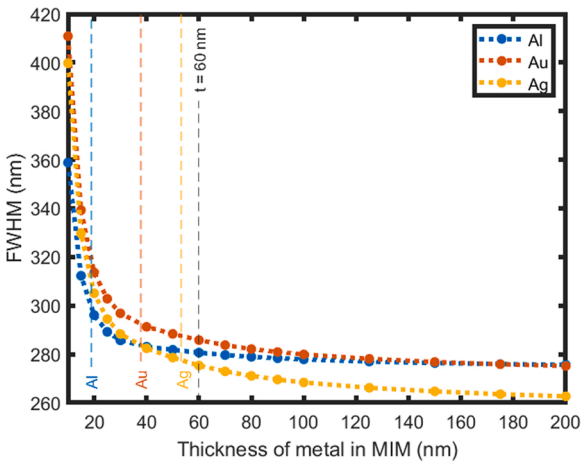

Fig. 2. The FWHM of metamaterial absorbers for the metals considered and as a function of the metal thickness, with the three colored dashed vertical lines indicating the electron mean path of the respective metal and the black dashed line the thickness used for the Al top layer.

tional to the electron mean free path, L_o. Values for the electron mean-free path of the materials considered here are $L_{o,Al} = 18.9nm$, $L_{o,Ag} = 53.3nm$, and $L_{o,Au} = 37.7nm$ [19] and indicate that L_o is shorter for Al as compared to Au or Ag. The bulk resistivities result as: $\rho_{o,Al} = 2.65\ \Omega.cm$, $\rho_{o,Ag} = 1.59\ \Omega.cm$, and $\rho_{o,Au} = 2.35\ \Omega.cm$. However, the electrical conductivity is significantly reduced for very thin metallic films, which is primarily due to the significant effect of electron scattering at the surface of the layer and at grain boundaries inside the film. According to the Mayadas-Shatzkes (MS) model, the resistivity of a film can be expressed as: $\rho/\rho_o = 1 + 2\alpha/3 + 3\alpha^2 - 3\alpha^3\ln(1 + 1/\alpha)$, with $\alpha = L_o/d_{grain} \times R_{grain}/(1 - R_{grain})$ where d_{grain} is the grain size and R_{grain} is the reflection coefficient at a grain boundary [20].

The value of R_{grain} depends on deposition conditions. A deposition technology that is optimized for small roughness is associated with a smaller grain size, which results in a smaller grain boundary reflection. Therefore, the resistivity of a thin film, ρ, strongly increases with the surface roughness [21]. The grain size also scales with layer thickness, t, according to a power law [22]. For thin layers, the grain size is almost equal to the thickness of the layer. As a consequence of all these uncertainties, a wide range of values has been reported in the literature for the metals considered.

Generally, the resistivity of the metallic film increases rapidly with reducing layer thickness for values smaller than the electron mean-free-path in the specific metal. For a top metal thickness of about 60*nm* the calculated peak absorption intensity does not significantly depend on the metal type used. Irrespective of metal type, the peak absorption is about $A = 1 - 2 \times 10^{-4}$ in case of a thickness in the range $40nm < t < 80nm$. Figure 2 shows the calculated bandwidth of the MIM structure as a function of metal thickness for the three metals considered. In this simulation, we assume $R_{grain} = 0.3$ for all three metals. The figure clearly indicates that the performance of a metasurface based on a MIM design with a 60*nm* Al top layer is very similar to the alternatives.

2.2. The use of CMOS dielectrics in metasurfaces

The complex refractive index of the dielectric layer, $n^* = n - jk$, is another important parameter of choice in the design of a mid-IR metamaterial. Several dielectrics are available in CMOS wafer-level fabrication that are in principle suitable for use in mid-IR metamaterials. The refractive index depends on the choice of material and deposition method and ranges from about n = 1 (airgap and porous layers) to $n = 1.5$ (SiO_2) and to $n > 2$ (oxynitride, Si_3N_4, SiC). Similar to the discussion on Al for use as the metal, the suitability of each of these CMOS compatible materials highly depends on the effect of fabrication tolerances in the thickness of the dielectric layer in the MIM stack on the optical performance of the resulting metasurface. SiO_2 is the most generic dielectric material in a CMOS process and often used in metamaterial design for the mid-IR.

Figure 3 a shows the spectral absorbance of a metasurface with disk-shaped Al patches as a function of the SiO_2 spacer thickness. The magnetic coupling between an electromagnetic wave and the metamaterial structure peaks at a thickness of about 180*nm*. As a consequence, the absorption peak increases to values close to unity at about 180*nm* spacer thickness. However, the bandwidth of the absorption peak increases marginally with a tolerance of $\pm$ 20*nm* around the optimal thickness of 180*nm*.

Figure 3b shows the absorber performance in case of a tolerance in layer thickness of $\pm$ 20*nm* (a specification of $\pm$ 10% is realistic in MEMS technology). The uncertainties in optical performance can be summarized as an uncertainty in peak absorbance of 0.01 and an uncertainty in wavelength of peak absorption of $\Delta\lambda/\lambda_o \sim 0.016$. Therefore, the

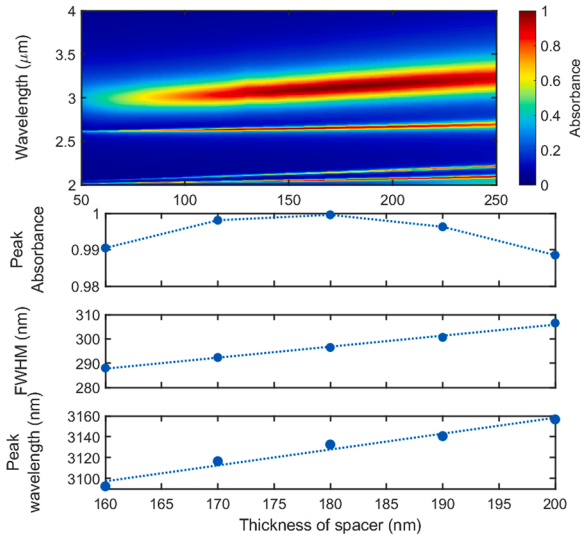

Fig. 3. (a) spectral absorbance of a metasurface with unit cells of a 3μm side-length and 1μm diameter Al circular patches as a function of the thickness of the dielectric layer, and variation of (b) peak absorbance, (c) FWHM, and (d) peak wavelength for a dielectric layer thickness in the range between 160 and 200*nm*.

tolerances in dielectric thickness have only a marginal effect on the metamaterial optical response.

From an intuitive argument one would expect that the optical thickness ($n \times t$) of the spacer must remain constant for avoiding a shift in the plasmonic resonance wavelength. Therefore, selecting a higher-index material for the dielectric spacer should be associated with a decrease in dielectric layer thickness. However, as shown in Figure 4, the resonance wavelength shifts linearly with increased index of refraction, n, towards longer wavelengths, even if a constant optical thickness is assured in the optical design. The shift toward longer wavelengths with increasing refractive index of the medium has been also observed and is the basis of many plasmonic refractive index sensors [23].

As the main challenge in metasurface design is to operate at an as short as possible wavelength at given minimum feature size of the technology, low-index materials are often preferred. The peak absorption in Figure 4 is maximum at about $n = 1.5$, because the thickness was optimized for the highest absorbance for SiO_2 ($n \sim 1.5$) with thickness of the dielectrics for other refractive index values scaled to a constant optical thickness ($1.5 \times 180 = 270nm$).

The dielectric loss due to the extinction coefficient (i.e. the imaginary part of the refractive index, k) does not contribute to the plasmonic resonance, but does affect the peak absorption and is a cause for widening of the absorption band. As shown in Figure 5, the plasmonic resonance is dominant up to $k \sim 10^{-2}$ and mainly results in a gradual increase in FWHM (lossy resonator). However, for values above $k \sim 10^{-1}$, the plasmonic resonance degrades, and dielectric losses dominate optical absorption. Therefore, a wideband response with somewhat moderated requirements on the peak absorption may be achieved by intentionally designing with a lossy dielectric material.

It can be concluded that the dielectric layers in a typical CMOS process are highly suitable for mid-IR metasurface design. The range of thicknesses in a typical mid-IR MIM design is very similar to that of layers deposited in microelectronic fabrication. For narrowband design the extinction coefficient should be limited to $k \sim 10^{-2}$.

2.3. Shape-tolerant metamaterial design

The masked fabrication used for enabling high throughput in CMOS batch fabrication inevitably results in a lower resolution as compared to high-resolution e-beam lithography. The consequence is a reduced control over the features reproduced from the mask into the photoresist, which ultimately results in shape deformations and deviations from the nominal dimensions of the sub-resolution patterns within the unit cell. Uncertainties, such as variations in the disk diameter of a circular patch, or irregularities in the shape, such as rounding of sharp corners in a cross-shaped patch, result in uncertainties in the spectral response of the absorber and thus in deviations from the target specifications used in the design. The limitations considered are minimum feature size and horizontal-vertical bias (HV bias).

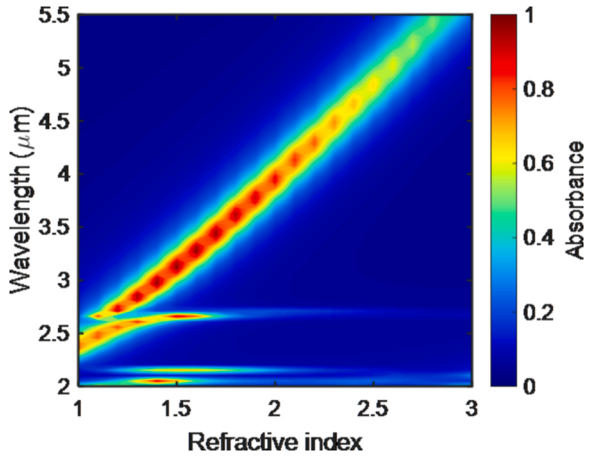

Fig. 4. Resonance wavelength shifts with spacer refractive index at a constant optical thickness of $n \times t = 270nm$.

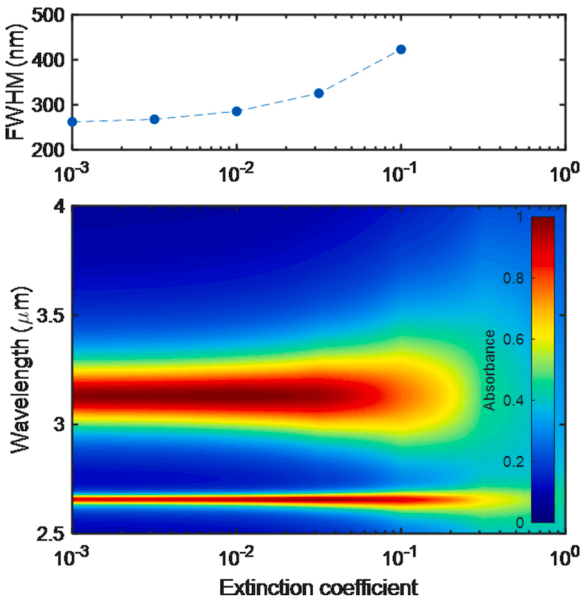

Fig. 5. (a) FWHM and (b) absorbance of a MIM vs. extinction coefficient in the dielectric layer.

2.3.1. Minimum feature size

The minimum feature size of the lithography is generally considered the most-essential parameter in micro-electronic fabrication, and this is indeed also the limiting factor in the fabrication of metamaterial absorbers for the mid-infrared spectrum. Figure 6a shows the simulated spectral absorbance of an aluminium wire patch metamaterial absorber with a length of 1000*nm* along the E-field, while the width of the wire is varied in the range between 500*nm* and 1000*nm*. At 1000*nm* width, the nanowire is basically transformed into a square patch. The thickness of the spacer and the patterned aluminium layer are kept constant in all simulations. Accordingly, for a perfectly patterned nanowire with sharp corners, decreasing the width from 1000*nm* to 500*nm* decreases the bandwidth from $\Delta\lambda/\lambda_o = 0.094–0.086$ (from 336 to 300*nm*), while the resonance wavelength shifts towards shorter wavelengths. The sharp corners of an ideal wire pattern are challenging to realize reliably in optical lithography resulting in rounding of the corners. The diffraction of light is considered as one of the leading causes of loss in high spatial frequency details of a pattern resulting in a corner radius.

For the projection lithography system (the wafer stepper), the minimum feature size is in the order of λ/NA, where λ and NA are the wavelength and numerical aperture of the lithography system. The corner radius can be estimated as about $\lambda/2NA$ [24]. Therefore, for a typical UV (i-line) lithography system, a corner radius of about 350*nm* can be calculated, which also implies that a feature size below $\lambda/NA \sim$ 700*nm* can in principle not be patterned.

The lower trace in Figure 6a indicates that the position of the absorption peak shows no dependence on the width of the wire in rounded corner wire design ($r = w/2$). This is confirmed by Figure 6b (peak absorbance at righthand endpoint of each of the curves is on a horizontal line). Figure 6b also indicates that increasing the corner radius from 150*nm* to 350*nm* results in a shift of the resonance wavelength towards shorter wavelengths, irrespective of width, while the FWHM reduces only for a width up to 800*nm*. The FWHM of a nanowire with rounded corners (righthand endpoint of each of the curves) is smaller as compared to the sharp design (left-hand endpoints). Decreasing the

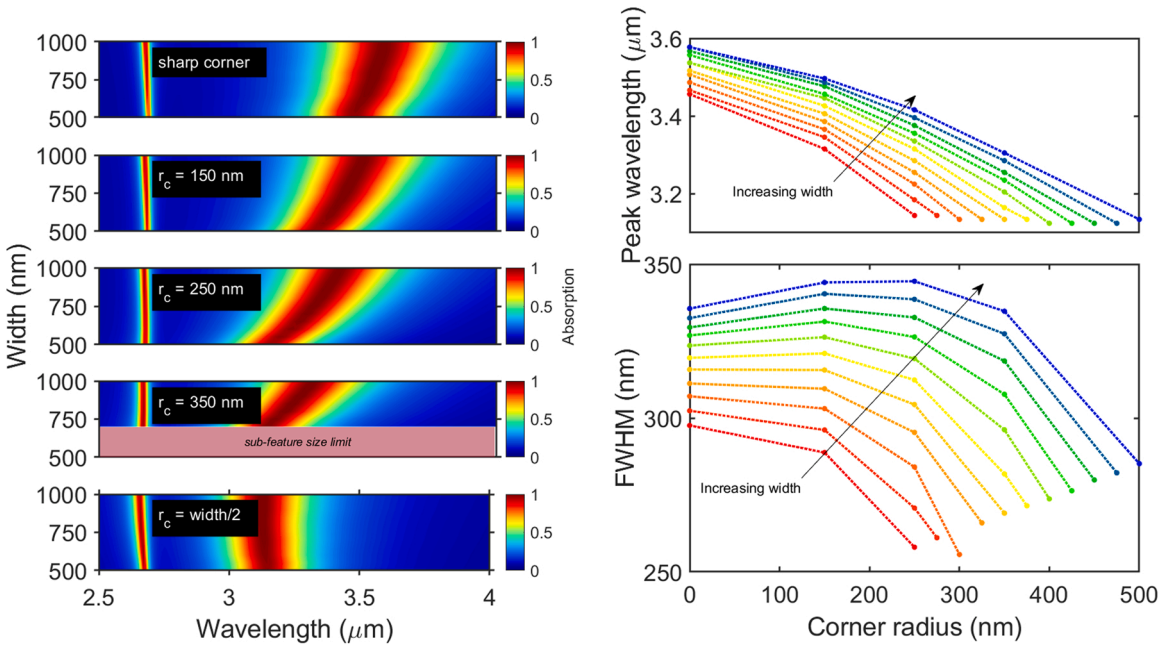

Fig. 6. (a) the spectral absorbance of a wire patch of 1000*nm* length and width in the range between 500*nm* and 1000*nm*, at different corner radii due to lithography, (b) the location of the peak absorbance and its FWHM, as a function of the corner radius and shown for the width in the range between 500*nm* and 1000*nm* in 50*nm* increments.

width of the wires generally results in a sharper peak in absorbance, which provides an incentive for the use of high-resolution lithography.

Therefore, intentionally designing a round nanowire with a corner radius of half of its width (a nanowire with circularly round ends) offers the best scenario: smallest FWHM (down to 280*nm*) with practically no resonance shift with variation in width, which is a compelling argument in favour of the circular patch.

2.3.2. *Horizontal-vertical bias*

A polarization dependency is removed in a symmetric MIM pattern. In some applications asymmetry is intentionally introduced to obtain multiple-band absorption [15,25]. Generally, symmetry is favoured, which brings the second limitation that is inherent to masked lithography of fine structures: the sensitivity to Horizontal-Vertical bias (HV bias), which results from astigmatism and aberrations in the lithography [26]. The result of HV bias is the distortion of a symmetric cross structure to a cross with unequal side-lengths (and width) or distortion of a circular pattern into an ellipse. Such distortions generally result in a polarization dependency of the absorbance, as the absorption peak generally depends on the length of the pattern along the E field direction. Since any reduced symmetry of the pattern by distortion due to HV bias has the same effect, we limit the study to the direction perpendicular to the polarization.

The HV bias in a circular disk pattern results in an elliptical pattern. The diameter along the E field (L_1) is selected to be 1100*nm*, while the diameter along the perpendicular direction (L_2) is varied from 900 to 1100*nm*. The resulting deviation from the circle can be denoted as eccentricity, $\epsilon = \sqrt{1 - L_2/L_1}$ and is equivalent to an eccentricity between $\epsilon = 0$ (perfectly circular) and $\epsilon = \sqrt{2/11}$. Figure 7 shows the effect of eccentricity on the resonance wavelength and FWHM. The absorption peak shifts to longer wavelengths with increasing L_2/L_1 ratio. The variations for an eccentricity $\epsilon < 0.2$ (which is equivalent to a size variation up to 10*nm*) are negligible, but rapidly increase at larger deviations. The HV bias in a properly calibrated machine is less than 1%. The effect of this distortion can be disregarded for $\epsilon < \sqrt{1 - 990/1000} = 0.1$ in Figure 7. Therefore, it can be concluded that the resolution is the most significant source of shape distortion in i-line masked lithography.

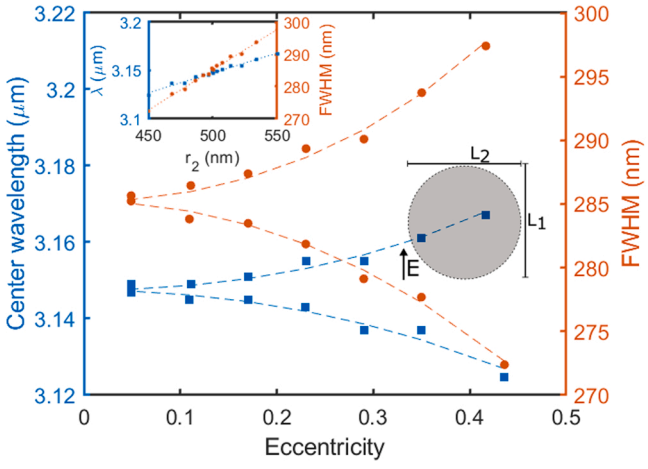

Fig. 7. Absorption spectra of metamaterial absorbers with a disk shaped Al patch. The diameter parallel to the electric field (L_1) is selected as 1000*nm*, and the perpendicular length (L_2) is varied from 900*nm* up to 1100*nm*. The thickness of the spacer layer for each metallic patch material is optimized to obtain maximum absorbance. The insert shows the center wavelength and FWHM as a function of $r_2 = L_2/2$.

3. Experimental validation and discussion

Based on the compatibility considerations discussed in previous sections, a metamaterial was designed for the spectral range between 3 and 4μm and based on an array of unit cells, as shown in Figure 8a. Arrays of unit cells are fabricated in three different designs of the circular patch; $D = 2r = 900nm$, 1000*nm*, and 1100*nm* diameter, each within a unit cell of side-line length $P = 3\mu m$. The nominal wavelengths of peak absorption are at 3200, 3420 and 3650*nm*, respectively.

Fabrication is based on silicon MEMS processing. Silicon wafers (4 in.) were used as the substrate. The Al layer that is normally deposited for use as the metal interconnect is used as the back plane of the metamaterial absorbers, which is basically a first step towards validation of

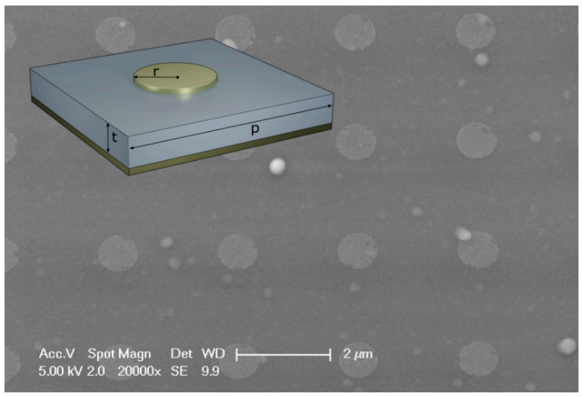

Fig. 8. (a) Structure of the unit cell of the metamaterial design with a circular metal patch with radius $r = 450 - 550nm$, unit cell side-length $P = 3\mu m$ and SiO_2 dielectric thickness $t = 170nm$. (b) SEM of the realized $r = 450nm$ metasurface.

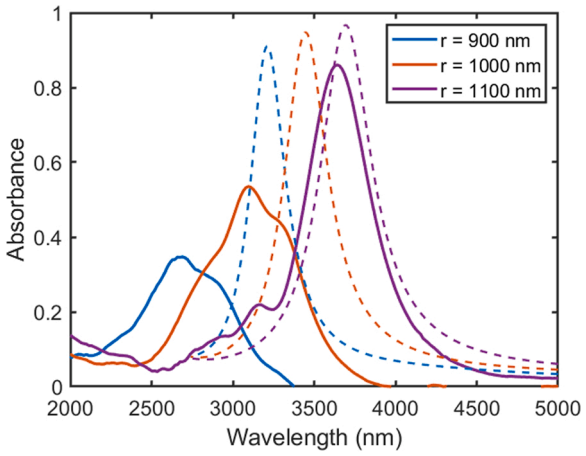

Fig. 9. Measured absorbance spectra for metamaterial patterns of different diameters as compared to theoretical expectations (dashed lines).

the CMOS compatibility. Subsequently, a 170*nm* PECVD TEOS-oxide film dielectric spacer is deposited at 350^oC. A lift-off process was used for the fabrication of the patch. A $1.5\mu m$ thick negative tone photoresist (nLOF 2020) was spin-coated and exposed using a wafer stepper (ASML; PAS5500/80). Following the development, an O_2 plasma step was applied for cleaning of the exposed surface area. Finally, a 60*nm* aluminium film was sputtered and followed by the lift-off process in NMP at 70^oC. The SEM of the fabricated structure of the 900*nm* diameter patch design is shown in Figure 8b. The SEM images of the three different designs were analysed using an image processing algorithm in MATLAB to extract statistical data for each absorber type. The circular patch design with a 900*nm* nominal diameter resulted in a distribution with an average diameter of 806*nm* and standard deviation of 32*nm*, while the design with 1000*nm* nominal results in a diameter distribution with an average of 888*nm* and a standard deviation of 24*nm*. Finally, the 1100*nm* nominal diameter resulted in a distribution with 1065*nm* average and a standard deviation of 17*nm*. The sample size used is a local cluster of 25 unit-cells.

The data indicates that the actual patch diameter is systematically smaller than its nominal value and that this error reduces with increased nominal diameter (− 11% for 900*nm* and − 3% for 1100*nm*), which is caused by the dependence of the feature size on exposure dose. Negative tone resist is used in combination with lift-off of the upper metal. Therefore, the patch area is defined by the non-exposed parts, which carries the risk of joining of non-exposed circular areas at minimum resolution (the 350*nm* half-linewidth of the UV i-line lithography). Although the exposure dose is kept as close as possible to the minimum of $40mJ/cm^2$ in an attempt to ensure that the transient exposed/non-exposed resist is not inside the area of patch definition for structures close to the resolution limit, the diameter of fabricated patches is smaller than nominal [11]. The relative effect is more profound in the smaller structures, which explains the reduced effect at increasing nominal patch diameter.

The IR absorbance of samples of metasurfaces of the three designs of nominal patch diameter was measured using an FTIR spectrometer (Bruker Vertex 70) equipped with a reflectance module. The absorbance results from the reflectance after calibration and assuming no transmission through the MIM array. The spectral measurements shown in Figure 9 are shifted to shorter wavelengths, which confirms the effects of distortions caused by the limited resolution of the lithography for especially the smaller structures. The spread in patch diameter is larger for the patches with a 900*nm* nominal diameter as compared to those of a 1100*nm* nominal diameter ($806 \pm 32nm$ versus $1065 \pm 17nm$) due to the larger relative effect of the reduced lithographic definition of structures with dimensions closer to the limits of the lithography. As the incident light illuminates a large number of unit cells, the overall absorption of the large-area absorber results from the combined effect of all these unit cells. The element-to-element variation results in many local spectral absorption curves that are not fully aligned and has resulted in a broadening of the overall absorption band with a reduced peak absorption in Figure 9. Note that the use of the Bruker reflectance unit results in the measurement at an angle of incidence of 12^o and not at normal incidence. In our earlier work we found only a minor effect for an angle of incidence up to 30^o [11].

High surface roughness in the metal layer was already discussed as a cause for low conductivity and a less profound plasmonic response. MIM absorbers with a high roughness have intentionally also been fabricated to compare the effect of roughness. Different techniques are available for SiO_2 deposition, each with a different optimum in terms of deposition rate and roughness of the final surface, which can conveniently be exploited in this experiment [27,28]. As shown in Figure 10, PECVD SiO_2 deposited at 400^oC results in a rougher surface as compared to PECVD TEOS deposited at 350^oC. Figure 10 also confirms that the rougher surface of PECVD SiO_2 ($Rq \sim 10nm$) results in an almost wavelength-independent absorbance, while PECVD TEOS ($Rq \sim 5nm$) results in a practically applicable spectral absorbance.

4. Conclusions

The definition of the features of metamaterial absorbers by masked lithography enables the on-chip fabrication of plasmonic devices at high

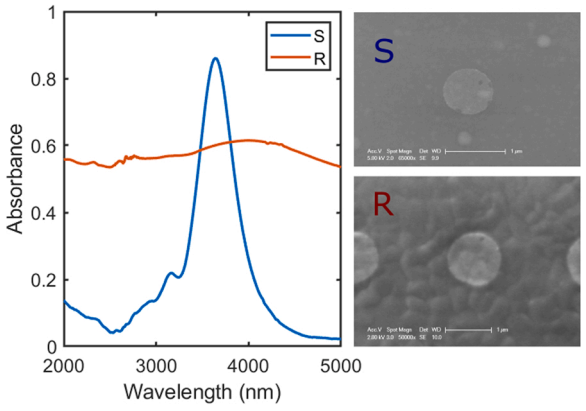

Fig. 10. Measured spectral absorbance of a metamaterial absorber with a diameter of 1100*nm* with metal patches on a SiO_2 dielectric layer deposited at different conditions resulting different roughness, as indicated in the SEMs: (S) PECVD TEOS: $Rq < 5nm$ and (R) PECVD Oxide ($Rq \sim 10nm$).

throughput and integration into CMOS-compatible MEMS, but also imposes several limitations. In this paper the consequences of this approach are discussed, along with their effects on the plasmonic response of a MIM-based absorber.

CMOS-compatibility of the absorber limits the number of acceptable materials. Although metamaterials are commonly fabricated using noble metals, these are not very suitable for CMOS-compatible integration. The CMOS-compatible metal Al was explored and was found fully acceptable for use as a MIM patch. The thin-film Al resistivity was found comparable to that of gold or silver at thin layers (thickness of about three times the electron mean free path in the material), despite the higher bulk resistivity, due to its shorter mean free path, and when including the loss in conductance due to grain boundary reflections.

The SiO_2 thin-film coatings that are ubiquitous in silicon microelectronics are also found highly suitable for MIM unit cell fabrication for mid-IR metamaterial-based absorbers. However, the result depends highly on the surface roughness of the deposited material. PECVD SiO_2 with a roughness $Rq \sim 10nm$ gave a poor result, while the use of a PECVD TEOS SiO_2 with $Rq < 5nm$ resulted in a spectral absorption that is close to the theoretical prediction.

The specifications of i-line UV lithography method, both in terms of resolution and HV bias, do limit the minimum feature size in the metamaterial design that can be reproducibly manufactured. The study of the effect of corner radius caused by the lithography process reveal that the rounded corners in a wire pattern typically cause uncertainty in resonance wavelength and FWHM. A design with corner radius equal to half the linewidth (which is a nanowire with circularly round ends) proved most resilient to these errors. This property comes automatically with a circular patch design. Therefore, it can be concluded that the circular patch is the most shape-tolerant design.

The study on HV bias has demonstrated that the distortion introduced by an HV bias of about 1% can be disregarded. Therefore, it can be concluded that the limitation of lithography are primarily due to resolution and HV bias is not further considered.

These theoretical findings have been validated using fabricated nanomaterials based on arrays of Al-SiO_2-Al MIM structures with top Al circular patches with a diameter of 900, 1000 or 1100nm. For the 170nm thick SiO_2 spacer and these values of the patch diameter, the nominal wavelengths of peak absorption are calculated at 3200, 3420 and 3650nm, respectively. Experimental results indicate reasonable agreement for the larger (1100nm diameter) structures. However, at a smaller patch diameter the systematic error and variations increase, which is due to the uncertainties introduced by the UV (i-line) lithography. The result is a shift of resonance wavelength, a significantly lowered peak absorption and an increased FWHM.

This work demonstrates that mid-IR metamaterial-based absorbers covering a chip area in excess of $0.1mm^2$ can be fabricated by masked lithography in a MEMS cleanroom environment. However, the spectral performance agrees well with simulation only for a design with peak absorption at a wavelength larger than about 3.5μm, while the surface roughness $Rq \sim 5nm$ limits the bandwidth to about $FWHM = 400nm$ in this particular design of the pattern. A split ring resonator can be designed to result in sharper peaks, however, is more susceptible to limitations of the mask lithography.

On-going work is on the design and fabrication using surface micromachining of a low-resolution MEMS microspectrometer for the mid-IR [29].

Declaration of Competing Interest

The authors declare that they have no known competing financial interests or personal relationships that could have appeared to influence the work reported in this paper.

Acknowledgements

This work was carried out at the EKL cleanroom of Delft University of Technology and is partly financially supported by the Dutch Research Council (NWO) domain Applied and Engineering Sciences (AES), project number DEL.11476 and also by ENIAC JU Project E450LMDAP Grant number 325613.

Author contributions

Both authors have equally contributed to the analysis and interpretation of results. Writing of the manuscript was mainly by RFW. Experimentation was mainly by MAG. Both authors have given approval to the final version.

References

[1] A. Li, S. Singh, D. Sievenpiper, Metasurfaces and their applications, Nanophotonics 7 (6) (2018) 989–1011.
[2] Y.P. Lee, J.Y. Rhee, Y.J. Yoo, K.W. Kim, Metamaterials for Perfect Absorption, vol. 236, Springer, 2016.
[3] X. Liu, T. Starr, A.F. Starr, W.J. Padilla, Infrared spatial and frequency selective metamaterial with near-unity absorbance, Phys. Rev. Lett. 104 (20) (2010), 207403.
[4] C.-W. Cheng, M.N. Abbas, C.-W. Chiu, K.-T. Lai, M.-H. Shih, Y.-C. Chang, Wide-angle polarization independent infrared broadband absorbers based on metallic multi-sized disk arrays, Opt. Express 20 (9) (2012) 10376–10381.
[5] A. Lochbaum, A. Dorodnyy, U. Koch, S.M. Koepfli, S. Volk, Y. Fedoryshyn, V. Wood, J. Leuthold, Compact mid-infrared gas sensing enabled by an all-metamaterial design, Nano Lett. 20 (6) (2020) 4169–4176.
[6] B.M. Adomanis, C.M. Watts, M. Koirala, X. Liu, T. Tyler, K.G. West, T. Starr, J. N. Bringuier, A.F. Starr, N.M. Jokerst, et al., Bi-layer metamaterials as fully functional near-perfect infrared absorbers, Appl. Phys. Lett. 107 (2) (2015), 021107.
[7] I. Faniayeu, V. Mizeikis, Realization of a helix-based perfect absorber for ir spectral range using the direct laser write technique, Opt. Mater. Express 7 (5) (2017) 1453–1462.
[8] S.H. Ahn, L.J. Guo, Large-area roll-to-roll and roll-to-plate nanoimprint lithography: a step toward high-throughput application of continuous nanoimprinting, ACS Nano 3 (8) (2009) 2304–2310.
[9] S. Bagheri, N. Strohfeldt, F. Sterl, A. Berrier, A. Tittl, H. Giessen, Large-area low-cost plasmonic perfect absorber chemical sensor fabricated by laser interference lithography, ACS Sens. 1 (9) (2016) 1148–1154.
[10] A. Lochbaum, Y. Fedoryshyn, A. Dorodnyy, U. Koch, C. Hafner, J. Leuthold, On-chip narrowband thermal emitter for mid-IR optical gas sensing, ACS Photonics 4 (6) (2017) 1371–1380.
[11] M. Ghaderi, E.K. Shahmarvandi, R.F. Wolffenbuttel, CMOS-compatible mid-ir metamaterial absorbers for out-of-band suppression in optical MEMS, Opt. Mater. Express 8 (7) (2018) 1696–1707.
[12] International roadmap for devices and systems (irds), 12.⟨https://irds.ieee.org/⟩, accessed: 2022–02-11.2022.
[13] W. Ma, Y. Wen, X. Yu, Broadband metamaterial absorber at mid-infrared using multiplexed cross resonators, Opt. Express 21 (25) (2013) 30724–30730.
[14] C. Meierbachtol, 2021. Permittivity of metals at optical wavelengths (Brendel-Bormann), MATLAB Central File Exchange, retrieved: 2021–06-10 (2021).
[15] T. Maier, H. Brueckl, Multispectral microbolometers for the midinfrared, Opt. Lett. 35 (22) (2010) 3766–3768.
[16] Z. Li, L. Stan, D.A. Czaplewski, X. Yang, J. Gao, Wavelength-selective mid-infrared metamaterial absorbers with multiple tungsten cross resonators, Opt. Express 26 (5) (2018) 5616–5631.
[17] R. Brendel, D. Bormann, An infrared dielectric function model for amorphous solids, J. Appl. Phys. 71 (1) (1992) 1–6.
[18] A.D. Rakić, A.B. Djurišić, J.M. Elazar, M.L. Majewski, Optical properties of metallic films for vertical-cavity optoelectronic devices, Appl. Opt. 37 (22) (1998) 5271–5283.
[19] D. Gall, Electron mean free path in elemental metals, J. Appl. Phys. 119 (8) (2016), 085101.
[20] A. Mayadas, M. Shatzkes, Electrical-resistivity model for polycrystalline films: the case of arbitrary reflection at external surfaces, Phys. Rev. B 1 (4) (1970) 1382.
[21] H. Marom, M. Eizenberg, The effect of surface roughness on the resistivity increase in nanometric dimensions, J. Appl. Phys. 99 (12) (2006), 123705.
[22] J.M. Camacho, A. Oliva, Surface and grain boundary contributions in the electrical resistivity of metallic nanofilms, Thin Solid Films 515 (4) (2006) 1881–1885.
[23] S. Sasi Brendel, S.M. Francis Bormann, J. Jacob, V.I. Thomas, A tunable plasmonic refractive index sensor with ultrabroad sensing range for cancer detection, Plasmonics 16 (5) (2021) 1705–1717.
[24] C.A. Mack, Corner rounding and line-end shortening in optical lithography. Microlithographic Techniques in Integrated Circuit Fabrication II, SPIE, 2000, pp. 83–92. Vol. 4226.
[25] K. Chen, R. Adato, H. Altug, Dual-band perfect absorber for multispectral plasmon-enhanced infrared spectroscopy, ACS Nano 6 (9) (2012) 7998–8006.

[26] J.J. Biafore, C.A. Mack, S.A. Robertson, M.D. Smith, S. Kapasi, The causes of horizontal-vertical (HV) bias in optical lithography: dipole source errors. Optical Microlithography XX, SPIE, 2007, pp. 1373–1390. Vol. 6520.

[27] M.R. Amirzada, A. Tatzel, V. Viereck, H. Hillmer, Surface roughness analysis of SiO_2 for PECVD, PVD and IBD on different substrates, Appl. Nanosci. 6 (2) (2016) 215–222.

[28] M. Ghaderi, G. De Graaf, R. Wolffenbuttel, Thermal annealing of thin PECVD silicon-oxide films for airgap-based optical filters, J. Micromech. Microeng. 26 (8) (2016), 084009.

[29] M.A. Ghaderi, P. Enoksson, R.F. Wolffenbuttel, CMOS compatible fabrication of mid infrared microspectrometers based on an array of metamaterial absorbers, In: 2019 20th International Conference on Solid-State Sensors, Actuators and Microsystems & Eurosensors XXXIII (TRANSDUCERS & EUROSENSORS XXXIII), IEEE, 2019, pp. 1580–1583.